

SCANET: A SELF- AND CROSS-ATTENTION NETWORK FOR AUDIO-VISUAL SPEECH SEPARATION

Kai Li¹, Runxuan Yang¹ & Xiaolin Hu^{1,2,3,*}

1. Department of Computer Science and Technology, Institute for AI, BNRIst, Tsinghua University, Beijing 100084, China

2. Tsinghua Laboratory of Brain and Intelligence (THBI),

IDG/McGovern Institute for Brain Research, Tsinghua University, Beijing 100084, China

3. Chinese Institute for Brain Research (CIBR), Beijing 100010, China

{1k21, yangrx20}@mails.tsinghua.edu.cn

xlhu@tsinghua.edu.cn

ABSTRACT

The integration of different modalities, such as audio and visual information, plays a crucial role in human perception of the surrounding environment. Recent research has made significant progress in designing fusion modules for audio-visual speech separation. However, they predominantly focus on multi-modal fusion architectures situated either at the top or bottom positions, rather than comprehensively considering multi-modal fusion at various hierarchical positions within the network. In this paper, we propose a novel model called *self- and cross-attention network (SCANet)*, which leverages the attention mechanism for efficient audio-visual feature fusion. SCANet consists of two types of attention blocks: self-attention (SA) and cross-attention (CA) blocks, where the CA blocks are distributed at the top (TCA), middle (MCA) and bottom (BCA) of SCANet. These blocks maintain the ability to learn modality-specific features and enable the extraction of different semantics from audio-visual features. Comprehensive experiments on three standard audio-visual separation benchmarks (LRS2, LRS3, and VoxCeleb2) demonstrate the effectiveness of SCANet, outperforming existing state-of-the-art (SOTA) methods while maintaining comparable inference time.

1 INTRODUCTION

In our daily lives, audio and visual signals are one of the primary means of information transmission, providing rich cues for humans to obtain valuable information in noisy environments (Cherry, 1953; Arons, 1992). This innate ability is known as the “cocktail party effect”, also referred to as “speech separation” in computer science. Speech separation possesses extensive research significance, such as assisting individuals with hearing impairments (Summerfield, 1992), enhancing the auditory experience of wearable devices (Ryumin et al., 2023), etc.

Researchers have previously sought to address the cocktail party effect through audio streaming alone (Luo & Mesgarani, 2019; Luo et al., 2020; Hu et al., 2021). However, the quality of the separation system may decline dramatically when speech is corrupted by noise (Afouras et al., 2018a). To address this issue, many researchers have focused on audio-visual speech separation (AVSS), achieving remarkable progress. Existing AVSS methods can be broadly classified into two categories based on their fusion modules: CNN-based and Transformer-based methods. CNN-based methods (Gao & Grauman, 2021; Li et al., 2022; Wu et al., 2019) exhibit lower computational complexity and excellent local feature extraction capabilities, enabling the extraction of audio-visual information at multiple scales to capture local contextual relationships. Transformer-based methods (Lee et al., 2021; Rahimi et al., 2022; Montesinos et al., 2022) can leverage self-attention mechanisms to learn associations across different time steps, effectively handling dynamic relationships between audio-visual information.

*Corresponding author.

By comparing the working mechanisms of these AVSS methods and the brain, we find that there are two major differences. First, visual and auditory information undergoes neural integration at multiple levels of the visual and auditory pathways, including the thalamus (Halverson & Freeman, 2006; Cai et al., 2019), A1 and V1 (Mesik et al., 2015; Eckert et al., 2008), and occipital cortex (Ghazanfar & Schroeder, 2006; Stein & Stanford, 2008). However, most AVSS methods only at coarse (Gao & Grauman, 2021; Lee et al., 2021) or fine (Li et al., 2022; Montesinos et al., 2022; Wu et al., 2019; Rahimi et al., 2022) temporal scales, thus ignoring semantic associations at different scales.

Second, numerous evidences have indicated that the brain employs selective attention to focus on relevant speech in a noisy environment (Cherry, 1953; Columbic et al., 2013). This also modulates neural responses in a frequency-specific manner, enabling the tracked speech to be distinguished and separated from competing speech (Columbic et al., 2013; Mesgarani & Chang, 2012; O’sullivan et al., 2015; Kaya & Elhilali, 2017; Cooke & Ellis, 2001; Aytar et al., 2016). The Transformer-based AVSS methods adopt attentional mechanisms (Rahimi et al., 2022; Montesinos et al., 2022), but they commonly employ Transformer as the backbone network to extract and fuse audio-visual features and the attention is not explicitly designed for selecting speakers. Some approaches (Chen et al., 2023; Kadandale et al., 2022) have used Transformer structures as their fusion modules, but the modules inevitably increase the computational cost due to the use of affinity matrices to calculate attention, thus limiting the practical application of these methods. In contrast to these complex fusion strategies, our approach aims to design a simple and efficient fusion module based on the selective attention mechanism.

To achieve this goal, inspired by the structure and function of the brain, we propose a novel, concise, and efficient audio-visual fusion scheme, called Self- and Cross-Attention¹ Network (SCANet), which leverages self- and cross-attention to extract diverse semantics from audio-visual features. SCANet consists of two types of attention blocks: self-attention (SA) (Li et al., 2023) and cross-attention (CA) blocks, where the CA blocks are distributed at the top (TCA), middle (MCA) and bottom (BCA) of SCANet. The SA blocks enhance unimodal contextual information, while the CA blocks combine auditory and visual features to associate the target sound source with visual content. The biological plausibility of these attention blocks is discussed in Conclusion and Discussion section.

On three AVSS benchmarks, we found that SCANet surpassed the previous SOTA method CTCNet (Li et al., 2022) by a considerable margin, while the model inference time was nearly on par with CTCNet. We also built a fast version of SCANet, termed SCANet-fast. It achieved an inference speed on CPU that was more than twice as fast as CTCNet and still yielded better separation quality on three datasets.

2 RELATED WORK

2.1 AUDIO-ONLY SPEECH SEPARATION

Audio-only speech separation (AOSS) is one of the many challenging speech enhancement tasks. Recently, speech separation methods have attracted the interest of researchers (Luo & Mesgarani, 2019; Hu et al., 2021; Li & Luo, 2022). Since the Transformer is leveraged in AOSS tasks, significant quality breakthroughs have been achieved. DPTNet (Chen et al., 2020) and Sepformer (Subakan et al., 2021) utilized Transformer layers to replace the RNN in DualPathRNN (Luo et al., 2020) for modeling local and global information. However, these methods introduce large computational complexity by incorporating Transformer layers, leading to long training and inference time. Recently, this problem has been alleviated in A-FRCNN (Hu et al., 2021) and TDANet (Li et al., 2023), which employ encoder-decoder architecture with recurrent connections and top-down attention, reducing model computational cost while maintaining quality. However, their separation quality in noisy scenarios is still inferior to AVSS methods that utilize visual cues.

¹Please note that here the self-attention and cross-attention are irrelevant to Transformer.

2.2 AUDIO-VISUAL SPEECH SEPARATION

Incorporating different modalities aligns better with the brain’s processing (Calvert, 2001; Bar, 2007). Some methods (Gao & Grauman, 2021; Li et al., 2022; Wu et al., 2019; Lee et al., 2021; Rahimi et al., 2022; Montesinos et al., 2022) have attempted to add visual cues in the AOSS task to improve the clarity of separated audios, called audio-visual speech separation (AVSS). They have demonstrated impressive separation results in more complex acoustic environments, but these methods only focus on audio-visual features fusion at a single temporal scale in both modality, e.g., only at the finest (Wu et al., 2019; Li et al., 2022; Rahimi et al., 2022; Montesinos et al., 2022) and coarsest (Gao & Grauman, 2021; Lee et al., 2021) scales, which restrains their efficient utilization of different modalities’ information. While CTCNet’s fusion module (Li et al., 2022) attempts to improve separation quality by utilizing visual and auditory features at different scales, it still focuses on fusion at the finest temporal scales. This unintentionally hinders the effectiveness of using visual information for guidance during the separation process. Moreover, some of the AVSS models (Lee et al., 2021; Sterpu et al., 2018; Cheng et al., 2023) employ attention mechanisms within the process of cross-modal fusion, while the significance of intra-modality attention mechanisms is overlooked. This deficiency constrains their separation capabilities, as the global information within the auditory modality plays a crucial role in enhancing the clarity of the separated audio (Li et al., 2023). Notably, the fusion module of these methods (Lee et al., 2021; Sterpu et al., 2018; Cheng et al., 2023) tend to use a similarity matrix to compute the attention signal, which not only dramatically increases the computational complexity of the fusion module but also increases the training and inference time of the model. In contrast, our proposed SCANet efficiently uses both intra-modality attention and cross-modal attention at different temporal scales.

2.3 ATTENTION MECHANISM IN THE BRAIN

Attention mechanism refers to the brain’s ability to selectively focus on a portion of information from multiple or single sensory inputs while ignoring other irrelevant information (Foxe & Snyder, 2011; Näätänen, 1990). Although it is widely believed that the interaction between attention mechanism and multisensory integration enables animals to separate and recombine mixed audio, researchers have yet to clearly understand the impact of attention mechanism between multisensory and unisensory processing stages (Alsius & Soto-Faraco, 2011; Mozolic et al., 2008; Klemen & Chambers, 2012). Recently, Kuo et al. (Kuo et al., 2022) constructed artificial neural networks to simulate the attention mechanism of auditory features, confirming that attention signals play a more critical role in addressing the cocktail party problem. However, the attention signal is from an extra source (the target speakers’ auditory features), which is unavailable in practical speech separation tasks. In addition, that work considered the role of attention signals in a single modality and were unclear about the impact of cross-modal attention mechanisms on solving the cocktail party problem.

3 THE PROPOSED MODEL

Let $\mathbf{A} \in R^{1 \times T_a}$ and $\mathbf{V} \in R^{H \times W \times T_v}$ represent the audio and video streams of an individual speaker, respectively, where T_a denotes the audio length; H , W , and T_v denote the height, width, and the number of lip frames, respectively. We aim to separate a high-quality, clean single-speaker audio \mathbf{A} from the noisy speech $\mathbf{S} \in R^{1 \times T_a}$ based on the video cues \mathbf{V} and filter out the remaining speech components (other interfering speakers). Specifically, our pipeline consists of four modules: audio encoder, video encoder, separation network and audio decoder (see Figure 1A).

The overall pipeline of the SCANet is summarized as follows. First, we obtain a video containing two speakers from the streaming media, and the lips are extracted from each image frame. Second, we encode the lip frames and noisy speech into lip embeddings $\mathbf{E}_V \in R^{N_v \times T_v}$ and noisy speech embeddings $\mathbf{E}_S \in R^{N_a \times T'_a}$ using a video encoder consistent with CTCNet (Li et al., 2022) and an audio encoder (one 1D convolutional layer), respectively, where N_v , N_a and T'_a are the visual and audio embedding dimensions and the number of audio frames, respectively. Third, the separation network takes \mathbf{E}_S and \mathbf{E}_V as inputs and outputs a soft mask $\mathbf{M} \in R^{N_a \times T'_a}$ for the target speaker. We multiply \mathbf{E}_S with \mathbf{M} to produce the target speaker’s speech embedding ($\bar{\mathbf{E}}_S = \mathbf{E}_S \odot \mathbf{M}$), where “ \odot ” denotes the element-wise product. Finally, we utilize the audio decoder (one 1D transposed

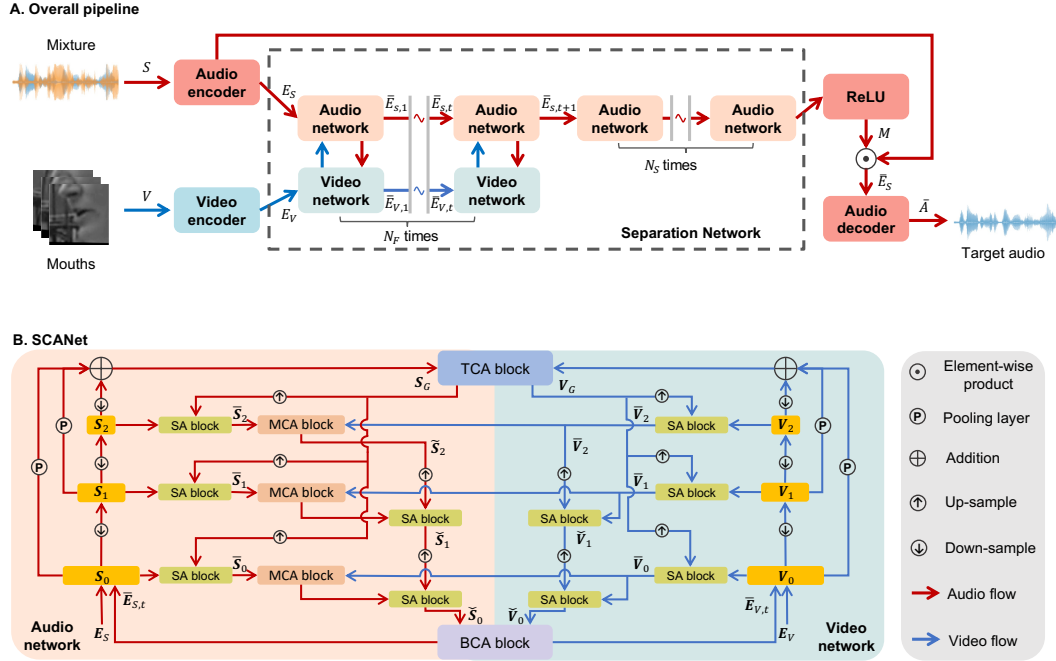


Figure 1: The overall pipeline of SCANet for audio-visual speech separation. (A) SCANet consists of four main components: audio encoder, video encoder, separation network, and audio decoder. (B) The separation network contains two attention blocks: SA and CA (TCA, MCA, BCA) blocks, denote the detailed architectures of the separation network in SCANet. The red and blue solid lines indicate the flow of auditory and visual features. The red and blue wavy lines indicate that the same module is repeated several times. All blocks use different parameters but keep the same across different cycles.

convolutional layer) to convert the $\bar{\mathbf{E}}_S$ back to the time domain, generating the target speaker’s speech $\bar{\mathbf{A}} \in R^{1 \times T_a}$.

3.1 AUDIO-VISUAL SEPARATION NETWORK

The core architecture of SCANet is an audio-visual separation network consisting of two types of components: (A) self-attention (SA) blocks, (B) cross-attention (CA) blocks (distributed at different locations: top (TCA), middle (MCA) and bottom (BCA)). The architecture of the separation network is illustrated in Figure 1B, which is described as follows:

1. **Bottom-up pass.** The auditory and visual networks take \mathbf{E}_S and \mathbf{E}_V as inputs and output multi-scale auditory $\{\mathbf{S}_i \in R^{N_a \times \frac{T_a'}{2^i}} | i = 0, 1, \dots, D\}$ and visual $\{\mathbf{V}_i \in R^{N_v \times \frac{T_v}{2^i}} | i = 0, 1, \dots, D\}$ features, where D denotes the total number of convolutional layers with a kernel size of 5 and a stride of 2, followed by a global normalization layer (GLN) (Luo & Mesgarani, 2019). In Figure 1B, we show an example model with $D = 2$.
2. **AV fusion through the TCA block.** The multi-scale auditory \mathbf{S}_i and visual \mathbf{V}_i features are fused using the TCA block (Figure 2A) at the top to obtain the cross-modal global features $\mathbf{S}_G \in R^{N_a \times \frac{T_a'}{2^D}}$ and $\mathbf{V}_G \in R^{N_v \times \frac{T_v}{2^D}}$.
3. **AV fusion in the top-down pass through SA and MCA blocks.** Firstly, the \mathbf{S}_G and \mathbf{V}_G are employed to modulate \mathbf{S}_i and \mathbf{V}_i within each modality using top-down SA blocks (Figure 2B) (Li et al., 2023), yielding auditory $\bar{\mathbf{S}}_i \in R^{N_a \times \frac{T_a'}{2^i}}$ and visual $\bar{\mathbf{V}}_i \in R^{N_v \times \frac{T_v}{2^i}}$ features. Secondly, the MCA block takes the auditory $\bar{\mathbf{S}}_i$ and visual $\bar{\mathbf{V}}_i$ features at the same scale as inputs, and output the modulated auditory features $\tilde{\mathbf{S}}_i \in R^{N_a \times \frac{T_a'}{2^i}}$ (Figure 2C).

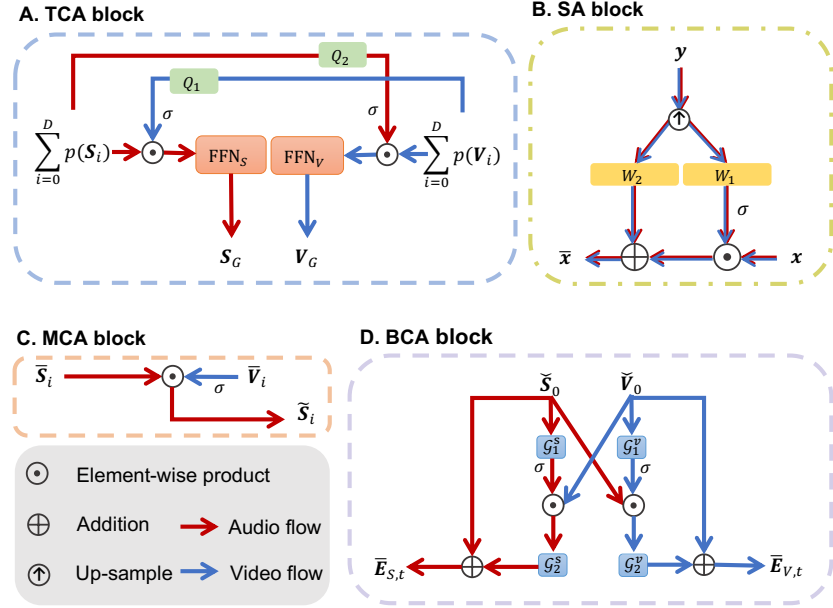


Figure 2: Flow diagram of CA blocks: (A) TCA block, (C) MCA block and (D) BCA block and (B) self-attention (SA) block in the SCANet, where \odot denotes element-wise product, $p(\cdot)$ denotes the average pooling layer and σ denotes the sigmoid function.

Finally, the top-down pass generates the auditory $\check{\mathbf{S}}_0 \in R^{N_a \times T'_a}$ and visual $\check{\mathbf{V}}_0 \in R^{N_v \times T_v}$ features at the maximum temporal scale.

4. **AV fusion through the BCA block.** The BCA block (Figure 2D) takes the auditory $\check{\mathbf{S}}_0$ and visual $\check{\mathbf{V}}_0$ features as input and outputs audio-visual features $\bar{\mathbf{E}}_{S,t} \in R^{N_a \times T'_a}$ and $\bar{\mathbf{E}}_{V,t} \in R^{N_v \times T_v}$, where t denotes the cycle index of audio-visual fusion.
5. **Cycle of audio and video networks.** The above steps complete the first cycle of the separation network. For the t -th cycle where $t \geq 2$, the audio-visual features $\bar{\mathbf{E}}_{S,t-1}$ and $\bar{\mathbf{E}}_{V,t-1}$ obtained in the $(t-1)$ -th cycle, instead of \mathbf{E}_S and \mathbf{E}_V , serve as input to the separation network, and we repeat the above steps. After N_F cycles, the auditory features $\bar{\mathbf{E}}_{S,t}$ are refined alone for N_S cycles in the audio network. Finally, we pass the output of the final cycle through an activation function (ReLU) to yield the separation network's output \mathbf{M} , as illustrated in Figure 1A.

The steps 2-4 and the blocks mentioned in these steps are described in details in what follows.

AV fusion through the TCA block. In the TCA block, we first utilize an average pooling layer to down-sample the temporal dimensions of \mathbf{S}_i and \mathbf{V}_i to $\frac{T'_a}{2^D}$ and $\frac{T_v}{2^D}$, respectively, and then merge them to obtain global features \mathbf{S}_G and \mathbf{V}_G using TCA block (Figure 2A). The detailed process of TCA block is described by the equations below:

$$\begin{aligned} \mathbf{S}_G &= \text{FFN}_S \left(\left(\sum_{i=0}^D p_i(\mathbf{S}_i) \right) \odot \sigma \left(Q_1(\mu(\sum_{i=0}^D p_i(\mathbf{V}_i))) \right) \right), \\ \mathbf{V}_G &= \text{FFN}_V \left(\left(\sum_{i=0}^D p_i(\mathbf{V}_i) \right) \odot \sigma \left(Q_2(\mu(\sum_{i=0}^D p_i(\mathbf{S}_i))) \right) \right), \end{aligned} \quad (1)$$

where $\text{FFN}(\cdot)$ denotes a feed-forward network with three convolutional layers followed by the GLN, Q_k denotes one convolutional layer followed by the GLN, $p_i(\cdot)$ denotes the average pooling layers, $\mu(\cdot)$ denotes interpolation up-sampling and σ denotes the sigmoid function. Here $p_i(\cdot)$ uses different pooling ratios for different i such that the temporal dimensions of all $p_i(\mathbf{S}_i)$ are $\frac{T'_a}{2^D}$ and the temporal dimensions of all $p_i(\mathbf{V}_i)$ are $\frac{T_v}{2^D}$. The hyperparameters of μ are specified such that the resulted audio

and video signals have the same temporal dimension. The hyperparameters of Q_k are specified such that the resulted audio and video signals have the same embedding dimension. The σ function receiving information from one modality acts as attention, modulating the other modality. The global features \mathbf{S}_G and \mathbf{V}_G are designed to guide the separation process in the two-down pass. Here we let them modulate each other and output useful information for this task.

AV fusion in the top-down pass through SA and MCA blocks. Given the multi-scale audio-visual features $\{\mathbf{S}_i, \mathbf{V}_i\}$ and \mathbf{S}_G and \mathbf{V}_G as inputs, we employ the self-attention (SA) blocks $\phi(\mathbf{x}, \mathbf{y})$ (Figure 2B) to extract audio $\bar{\mathbf{S}}_i$ and visual features $\bar{\mathbf{V}}_i$ at each temporal scale,

$$\bar{\mathbf{x}} = \phi(\mathbf{x}, \mathbf{y}) = \sigma(W_1(\mu(\mathbf{y}))) \odot \mathbf{x} + W_2(\mu(\mathbf{y})) \quad (2)$$

where $W_k(\cdot)$ denote one 1D convolutional layer followed by the GLN. Same as in (1), the hyperparameters of W_k and μ are specified such that the element-wise product and addition in (2) function correctly. It is named *self-attention* in this paper to emphasize that the attention signal \mathbf{y} is from the same modality as \mathbf{x} . This function has played a significant role in AOSS (Li et al., 2023). For audio signals, $\bar{\mathbf{S}}_i = \phi(\mathbf{S}_i, \mathbf{S}_G)$; for video signals, $\bar{\mathbf{V}}_i = \phi(\mathbf{V}_i, \mathbf{V}_G)$.

In contrast to previous AVSS methods (Gao & Grauman, 2021; Li et al., 2022), we investigate which part of the audio network should be attended to undergo the guidance of visual features within the same temporal scale. We utilize the visual features $\bar{\mathbf{V}}_i$ from the same temporal scale as $\bar{\mathbf{S}}_i$ to guide auditory features $\bar{\mathbf{S}}_i$ using middle CA blocks (MCA blocks, Figure 2C), which can capture the correlation between auditory and visual features, and obtain the updated auditory features $\tilde{\mathbf{S}}_i \in R^{N \times \frac{T'_a}{2^i}}$:

$$\tilde{\mathbf{S}}_i = \sigma(F(\mu(\bar{\mathbf{V}}_i))) \odot \bar{\mathbf{S}}_i, \quad (3)$$

where $F(\cdot)$ denotes one 1D convolutional layer followed by the GLN. Same as before, the hyperparameters of F and μ are specified such that the two terms on the two sides of \odot have the same dimension. Compared to $\bar{\mathbf{S}}_i$, $\tilde{\mathbf{S}}_i$ retains intra-modal details and introduces inter-modal correlations. In this way the MCA blocks are expected to extract the target speaker’s sound features according to the target speaker’s visual features at the same scale.

Then, we reconstructed auditory and visual features separately to obtain the features $(\check{\mathbf{S}}_0, \check{\mathbf{V}}_0)$ in a top-down pass (Figure 1B). To achieve this, multi-scale features are continuously up-sampled from $(\check{\mathbf{S}}_{D-1}, \check{\mathbf{V}}_{D-1})$ to $(\check{\mathbf{S}}_0, \check{\mathbf{V}}_0)$ to obtain the finest-grained auditory $\check{\mathbf{S}}_0$ and visual features $\check{\mathbf{V}}_0$ using SA blocks. This process can be described as follows:

$$\begin{cases} \check{\mathbf{S}}_i = \phi(\tilde{\mathbf{S}}_i, \tilde{\mathbf{S}}_{i+1}) & \text{if } i = D-1, \\ \check{\mathbf{V}}_i = \phi(\tilde{\mathbf{V}}_i, \tilde{\mathbf{V}}_{i+1}) & \text{if } i < D-1, \end{cases} \quad (4)$$

Please note that different SA blocks within one cycle as depicted in Figure 1B use different parameters. In the top-down pass, we use SA blocks to fuse as many multi-scale features as possible while reducing information redundancy.

AV fusion through the BCA block. In CTCNet (Li et al., 2022), the global audio-visual features fused all auditory and visual multi-scale features using the concatenation strategy, leading to high computational complexity. Here, we only perform cross-modal fusion on the finest-grained auditory and visual features $(\check{\mathbf{S}}_0, \check{\mathbf{V}}_0)$, greatly reducing computational complexity.

Specifically, we reduce the impact of redundant features by incorporating the BCA block (Figure 2D) between the finest-grained auditory and visual features $\check{\mathbf{S}}_0$ and $\check{\mathbf{V}}_0$. In particular, the process of global audio-visual fusion is as follows:

$$\begin{aligned} \bar{\mathbf{E}}_{S,t} &= \check{\mathbf{S}}_0 + \mathcal{G}_2^s(\mu(\check{\mathbf{V}}_0) \odot \sigma(\mathcal{G}_1^s(\check{\mathbf{S}}_0))), \\ \bar{\mathbf{E}}_{V,t} &= \check{\mathbf{V}}_0 + \mathcal{G}_2^v(\mu(\check{\mathbf{S}}_0) \odot \sigma(\mathcal{G}_1^v(\check{\mathbf{V}}_0))), \end{aligned} \quad (5)$$

where $\mathcal{G}_k^j(\cdot)$ denotes one convolutional layer followed by the GLN. Same as in (1), the hyperparameters of \mathcal{G}_k^j and μ are specified such that the element-wise product and addition in (5) function correctly. The working process of this block is simple. One modality features are modulated by the other modality features through an attention function σ , then the results are added to the original features. Several convolutions and up-samplings are interleaved in the process to ensure that the

dimensions of results are appropriate. We keep the original features in the final results by addition because we do not want the final features to be altered too much by the other modality information.

Finally, the output auditory and visual features $\bar{\mathbf{E}}_{S,t}$ and $\bar{\mathbf{E}}_{V,t}$ serve as inputs for the subsequent auditory and visual networks.

4 EXPERIMENTS

4.1 DATASETS

Consistent with previous research, we experimented on three commonly used AVSS datasets: LRS2 (Afouras et al., 2018a), LRS3 (Afouras et al., 2018b), and VoxCeleb2 (Chung et al., 2018). Each audio is 2-second in length with a sampling rate of 16kHz. The mixture was created by randomly selecting two different speakers from datasets and mixing their speeches with signal-to-noise ratios between -5dB and 5dB. Lip frames were synchronized with audio, having a frame rate of 25 FPS and a size of 88×88 grayscale images. We used the same dataset split consistent with previous works (Li et al., 2022; Gao & Grauman, 2021; Lee et al., 2021).

LRS2 (Afouras et al., 2018a). The LRS2 dataset consists of thousands of BBC video clips, divided into Train, Validation, and Test folders. Since the LRS2 data contains reverberation and noise, and the overlap rate is not 100%, it is very close to a real-world scene.

LRS3 (Afouras et al., 2018b). The LRS3 dataset includes thousands of spoken sentences from TED and TEDx videos, divided into Trainval and Test folders. In contrast to LRS2, the LRS3 data has relatively less noise and is closer to separation tasks in clean environments.

VoxCeleb2 (Chung et al., 2018). The VoxCeleb2 dataset contains over one million sentences from 6,112 individuals extracted from YouTube videos, divided into Dev and Test folders. Similar to LRS2, VoxCeleb2 also contains a significant amount of noise and reverberation, making it close to real-world scenarios, but the acoustic environment of VoxCeleb2 is more complex and challenging.

Model	LRS2		LRS3		VoxCeleb2	
	SI-SNRI	SDRi	SI-SNRI	SDRi	SI-SNRI	SDRi
AVConvTasNet (Wu et al., 2019)	12.5	12.8	11.2	11.7	9.2	9.8
Visualvoice (Gao & Grauman, 2021)	11.5	11.8	9.9	10.3	9.3	10.2
CaffNet-C (Lee et al., 2021)	-	10.0	-	9.8	-	7.6
AVLiT-8 (Martel et al., 2023)	12.8	13.1	13.5	13.6	9.4	9.9
CTCNet (Li et al., 2022)	14.3	14.6	17.4	17.5	11.9	13.1
SCANet-fast (<i>ours</i>)	15.4	15.7	17.8	17.9	12.6	13.6
SCANet (<i>ours</i>)	16.4	16.6	18.3	18.5	14.0	15.1

Table 1: Separation results of different AVSS methods on LRS2, LRS3, and VoxCeleb2 datasets. These metrics represent the average values for all speakers in each test set, where larger SI-SNRI and SDRi values are better. “-” denotes results not reported in the original paper.

Methods	Computation Cost		Inference Time		GPU Memory (MB)
	MACs (G/s)	Params (M)	CPU (s)	GPU (ms)	
Visualvoice	9.7	77.8	2.98	110.31	313.74
AVConvTasNet	23.8	16.5	1.06	62.51	117.05
AVLiT	23.8	16.5	0.46	62.51	24.0
CTCNet	167.1	7.0	1.26	84.17	75.8
SCANet-fast (<i>ours</i>)	11.9	3.1	0.52	70.94	12.5
SCANet (<i>ours</i>)	18.6	3.1	1.27	110.11	12.5

Table 2: Parameter sizes and computational complexities of different AVSS methods. All results are measured with an input audio length of 1 second, a sampling rate of 16 kHz, and a video frame sampling rate of 25 FPS. Inference time is measured in the same testing environment without the use of any additional acceleration techniques, such as quantization or pruning.

4.2 MODEL CONFIGURATIONS AND EVALUATION METRICS

The SCANet model was implemented using PyTorch (Paszke et al., 2019), and optimized using the Adam optimizer (Kingma & Ba, 2014) with an initial learning rate of 0.001. The learning rate was cut by 50% whenever there was no improvement in the best validation loss for 15 consecutive epochs. The training was halted if the best validation loss failed to improve over 30 successive epochs. Gradient clipping was used during training to avert gradient explosion, setting the maximum L_2 norm to 5. We used SDR losses to train SCANet, see Appendix B for details. All experiments were conducted with a batch size of 6, utilizing 8 Tesla 80 GB A100 GPUs. The hyperparameters are included in Appendix A.

Same as previous research (Gao & Grauman, 2021; Li et al., 2022; Afouras et al., 2018a), the SDRi (Vincent et al., 2006) was used as a metric for speech separation. In addition, the SI-SNRI (Le Roux et al., 2019) was employed to assess speech quality, removing the influence of energy on the quality assessment.

4.3 COMPARISONS WITH STATE-OF-THE-ART METHODS

To explore the efficiency of the proposed approach, we have designed a faster version, namely SCANet-fast, which runs half of N_S cycles compared to SCANet (see Appendix A for detailed parameters). We compared SCANet and SCANet-fast with existing AVSS methods. To conduct a fair comparison, we obtained metric values in original papers or reproduced the results using officially released models by the authors.

Separation quality. As demonstrated in Table 1, SCANet consistently outperformed existing methods across all datasets, with at least a 0.9dB gain in SI-SNRI. In particular, SCANet excelled in complex environments, notably on the LRS2 and VoxCeleb2 datasets, outperforming AVSS methods by a minimum of 1.5 dB SI-SNRI in separation quality. In addition, SCANet-fast also achieved SOTA results. This significant improvement highlights the power of SCANet in audio-visual fusion.

Model size and computational cost. In practical applications, model size and computational cost are often crucial considerations. We employed three hardware-agnostic metrics to circumvent disparities between different hardware, including number of parameters (Params) and Multiply-Accumulate operations (MACs)², and GPU memory usage during inference. Furthermore, we also selected two hardware-related metrics to test inference speed on specific GPU and CPU hardware. The results were shown in Table 2. We found that SCANet was slower in inference than the previous SOTA method CTCNet, but SCANet had a smaller memory footprint and achieved best audio quality. This is because the top-down inference of CTCNet can be completed in a single step, whereas SCANet needs to be completed step-by-step, which will increase the inference time. SCANet-fast had less computational cost (only 7% of CTCNet’s MACs), and substantially faster inference speed (40% of CTCNet’s time on CPU and 84% of CTCNet’s time on GPU). Furthermore, SCANet-fast managed to surpass CTCNet in separation quality with an improvement of 1 dB in SI-SNRI on the LRS2 dataset. This not only showcased the efficiency of SCANet-fast but also highlighted its aptness for deployment onto environments with limited hardware resources and strict real-time requirement. In conclusion, compared to AVSS methods, SCANet achieved a relatively good trade-off between inference speed and separation quality.

4.4 ABLATION STUDY

To examine the effectiveness of different modules, we conducted ablation experiments on SA and proposed CA (TCA, MCA and BCA) blocks. These ablation experiments were trained and evaluated on the LRS2 dataset.

Importance of SA and CA. We investigated the role of SA and CA in model performance. To this end, we constructed a control model resulted from removing SA and CA blocks from SCANet. Basically, it uses UNet (Ronneberger et al., 2015) architecture as the visual and auditory backbones and fused visual and auditory features at the finest temporal scale (see Figure S1A). The training and

²For applications that need to run models in resource-constrained environments, such as mobile devices and edge computing, MACs are a key metric because they are directly related to power consumption, latency, and storage requirements.

inference procedures are the same as SCANet (Figure 1A). As shown in Table 3, adding SA blocks into the control model (see Figure S1B) significantly improved separation quality. Specifically, the SI-SNRI and SDRI metrics were improved by 0.5 dB and 0.6 dB. This improvement validated the effectiveness of the SA blocks in the AVSS task, though it was originally proposed for AOSS (Li et al., 2023). We then added the CA blocks to the model (see Figure 1B). We found that the model was able to obtain a substantial separation quality improvement by 2.8 dB and 2.6 dB in SI-SNRI and SDRI metrics respectively compared to the model containing only SA blocks. Taken together, the results show the effectiveness of the SA and CA blocks.

Model	SI-SNRI/SDRI	Params/MACs
Control model	13.1/13.4	2.2/16.65
Control model + SA	13.6/14.0	2.2/18.09
Control model + SA + CA (SCANet)	16.4/16.6	3.1/18.64

Table 3: Importance of SA blocks and CA blocks. MACs are measured with 1s input audio sampled at 16 kHz.

Comparison of different CA blocks. Table 4 reports the performances of different combinations of the three CA modules TCA, MCA and BCA. Please note that excluding TCA block means directly using $\sum_{i=0}^D p(\mathbf{S}_i)$ and $\sum_{i=0}^D p(\mathbf{V}_i)$ as input to auditory and visual MLPs, respectively, with cross-modal attention signal removed. Excluding MCA block means removing visual fusion branches at each temporal scale. Excluding BCA block means not performing fine-grained audio-visual fusion.

When only one of the attention modules is enabled in the inter-modal settings, the MCA block results in the highest separation quality. On this basis, by adding the MCA block to TCA and BCA blocks, we observe quality gains of 1.4 dB. It can provide same-scale audio and visual information for features at each scale and dynamically fuse audio-visual features to enhance the ability to reconstruct fine-grained features of the intra-modality.

TCA	MCA	BCA	SI-SNRI / SNRI	Params / MACs
✓	✗	✗	13.8 / 14.1	2.3 / 18.08
✗	✓	✗	14.5 / 14.7	2.7 / 17.97
✗	✗	✓	14.1 / 14.4	2.3 / 18.49
✓	✓	✗	14.8 / 15.1	3.0 / 18.10
✓	✗	✓	15.0 / 15.2	2.6 / 18.62
✗	✓	✓	15.5 / 15.7	2.8 / 18.51
✓	✓	✓	16.4 / 16.6	3.1 / 18.64

Table 4: Impact of each CA block in SCANet on the LRS2 test set. MACs are measured on 1-second input audio sampled at 16 kHz. Please note that, as SCANet is an AVSS method, it must include at least one of the three CA blocks.

4.5 QUALITATIVE EVALUATION

We evaluated different AVSS methods (AVConvTasNet, Visualvoice, CTCNet) in real-world scenarios by collecting multi-speaker videos on YouTube. Since these videos do not have ground truth separated audio, we can only perform a qualitative evaluation of the results. Some typical results are presented in Supplementary Materials. By listening to these results, one can confirm that SCANet generated higher-quality separated audio than other separation models.

5 CONCLUSION AND DISCUSSION

We proposed a brain-inspired AVSS model, which is characterized by extensive use of self-attention and cross-attention in the audio and video networks. Compared to the previous SOTA method CTCNet on three benchmark datasets, SCANet achieved significantly higher separation quality with

11% MACs, 44% paramers and 16% GPU memory. By reducing the number of cycles, SCANet ran much faster than CTCNet yet still obtain better results.

The human brain excels in solving the “cocktail party problem”. Though it remains a mystery how the brain solves the problem, many relevant structural and functional properties have been revealed. We believe that the following two specific properties play important roles in this process. First, both auditory and visual pathways have hierarchical structures, and the two pathways interact with each other at multiple stages in the pathways, e.g., the thalamus (Halverson & Freeman, 2006; Cai et al., 2019), the primary auditory and visual areas (Falchier et al., 2002; Rockland & Ojima, 2003) and higher-level association cortical areas, including the frontal cortex, occipital cortex, and temporal association cortex (Raij et al., 2000; Keil et al., 2012; Stein & Stanford, 2008). Second, the brain utilizes attention, manifesting in the form of neural modulation in physiological experiments (Mehta et al., 2000; Alho et al., 1994), to select information of interest. Prior works (Li et al., 2022; 2023) have taken some of these facts to design AVSS methods, but have missed certain critical features. The proposed SCANet integrates most of these neuroscience facts by introducing cross-attention (TCA, MCA and BCA blocks) between the audio network and video network at multiple stages. It is a more complete brain-inspired AVSS model, laying a framework for integrating more neuroscience facts to improve performance in the future.

REFERENCES

Triantafyllos Afouras, Joon Son Chung, Andrew Senior, Oriol Vinyals, and Andrew Zisserman. Deep audio-visual speech recognition. *IEEE Transactions on Pattern Analysis and Machine Intelligence*, 44(12):8717–8727, 2018a.

Triantafyllos Afouras, Joon Son Chung, and Andrew Zisserman. Lrs3-ted: a large-scale dataset for visual speech recognition, 2018b.

Kimmo Alho, David L Woods, and Alain Algazi. Processing of auditory stimuli during auditory and visual attention as revealed by event-related potentials. *Psychophysiology*, 31(5):469–479, 1994.

Agnès Alsius and Salvador Soto-Faraco. Searching for audiovisual correspondence in multiple speaker scenarios. *Experimental Brain Research*, 213:175–183, 2011.

Barry Arons. A review of the cocktail party effect. *Journal of the American Voice I/O Society*, 12 (7):35–50, 1992.

Yusuf Aytar, Carl Vondrick, and Antonio Torralba. Soundnet: Learning sound representations from unlabeled video. volume 29, 2016.

Moshe Bar. The proactive brain: using analogies and associations to generate predictions. *Trends in Cognitive Sciences*, 11(7):280–289, 2007.

Dongqin Cai, Yin Yue, Xin Su, Miaoqiao Liu, Yiwei Wang, Ling You, Fenghua Xie, Fei Deng, Feng Chen, Minmin Luo, et al. Distinct anatomical connectivity patterns differentiate subdivisions of the nonlemniscal auditory thalamus in mice. *Cerebral cortex*, 29(6):2437–2454, 2019.

Gemma A Calvert. Crossmodal processing in the human brain: insights from functional neuroimaging studies. *Cerebral Cortex*, 11(12):1110–1123, 2001.

Jiaben Chen, Renrui Zhang, Dongze Lian, Jiaqi Yang, Ziyao Zeng, and Jianbo Shi. iquery: Instruments as queries for audio-visual sound separation. In *Proceedings of the IEEE/CVF Conference on Computer Vision and Pattern Recognition*, pp. 14675–14686, 2023.

Jingjing Chen, Qirong Mao, and Dong Liu. Dual-path transformer network: Direct context-aware modeling for end-to-end monaural speech separation. In *Annual Conference of the International Speech Communication Association*. ISCA, 2020.

Haoyue Cheng, Zhaoyang Liu, Wayne Wu, and Limin Wang. Filter-recovery network for multi-speaker audio-visual speech separation. In *International Conference on Learning Representations*, 2023.

E Colin Cherry. Some experiments on the recognition of speech, with one and with two ears. *The Journal of the Acoustical Society of America*, 25(5):975–979, 1953.

Joon Son Chung, Arsha Nagrani, and Andrew Zisserman. Voxceleb2: Deep speaker recognition, 2018.

Martin Cooke and Daniel PW Ellis. The auditory organization of speech and other sources in listeners and computational models. *Speech Communication*, 35(3-4):141–177, 2001.

Mark A Eckert, Nirav V Kamdar, Catherine E Chang, Christian F Beckmann, Michael D Greicius, and Vinod Menon. A cross-modal system linking primary auditory and visual cortices: Evidence from intrinsic fmri connectivity analysis. *Human brain mapping*, 29(7):848–857, 2008.

Arnaud Falchier, Simon Clavagnier, Pascal Barone, and Henry Kennedy. Anatomical evidence of multimodal integration in primate striate cortex. *Journal of Neuroscience*, 22(13):5749–5759, 2002.

John J Foxe and Adam C Snyder. The role of alpha-band brain oscillations as a sensory suppression mechanism during selective attention. *Frontiers in Psychology*, 2:154, 2011.

Ruohan Gao and Kristen Grauman. Visualvoice: Audio-visual speech separation with cross-modal consistency. In *2021 IEEE/CVF Conference on Computer Vision and Pattern Recognition (CVPR)*, pp. 15490–15500. IEEE, 2021.

Asif A Ghazanfar and Charles E Schroeder. Is neocortex essentially multisensory? *Trends in cognitive sciences*, 10(6):278–285, 2006.

Elana M Zion Golumbic, Nai Ding, Stephan Bickel, Peter Lakatos, Catherine A Schevon, Guy M McKhann, Robert R Goodman, Ronald Emerson, Ashesh D Mehta, Jonathan Z Simon, et al. Mechanisms underlying selective neuronal tracking of attended speech at a “cocktail party”. *Neuron*, 77(5):980–991, 2013.

Hunter E Halverson and John H Freeman. Medial auditory thalamic nuclei are necessary for eyeblink conditioning. *Behavioral neuroscience*, 120(4):880, 2006.

Xiaolin Hu, Kai Li, Weiyi Zhang, Yi Luo, Jean-Marie Lemercier, and Timo Gerkmann. Speech separation using an asynchronous fully recurrent convolutional neural network. volume 34, pp. 22509–22522, 2021.

Venkatesh S Kadandale, Juan F Montesinos, and Gloria Haro. Vocalist: An audio-visual synchronisation model for lips and voices, 2022.

Emine Merve Kaya and Mounya Elhilali. Modelling auditory attention. *Philosophical Transactions of the Royal Society B: Biological Sciences*, 372(1714):20160101, 2017.

Julian Keil, Nadia Müller, Niklas Ihssen, and Nathan Weisz. On the variability of the mcgurk effect: audiovisual integration depends on prestimulus brain states. *Cerebral Cortex*, 22(1):221–231, 2012.

Diederik P. Kingma and Jimmy Ba. Adam: A method for stochastic optimization, 2014.

Jane Klemen and Christopher D Chambers. Current perspectives and methods in studying neural mechanisms of multisensory interactions. *Neuroscience & Biobehavioral Reviews*, 36(1):111–133, 2012.

Ting-Yu Kuo, Yuanda Liao, Kai Li, Bo Hong, and Xiaolin Hu. Inferring mechanisms of auditory attentional modulation with deep neural networks. *Neural Computation*, 34(11):2273–2293, 2022.

Jonathan Le Roux, Scott Wisdom, Hakan Erdogan, and John R Hershey. Sdr-half-baked or well done? In *2019-2019 IEEE International Conference on Acoustics, Speech and Signal Processing*, pp. 626–630, 2019.

Jiyoung Lee, Soo-Whan Chung, Sunok Kim, Hong-Goo Kang, and Kwanghoon Sohn. Looking into your speech: Learning cross-modal affinity for audio-visual speech separation. In *Proceedings of the IEEE/CVF Conference on Computer Vision and Pattern Recognition*, pp. 1336–1345. IEEE, 2021.

Kai Li and Yi Luo. On the design and training strategies for rnn-based online neural speech separation systems. In *Annual Conference of the International Speech Communication Association*. ISCA, 2022.

Kai Li, Fenghua Xie, Hang Chen, Kexin Yuan, and Xiaolin Hu. An audio-visual speech separation model inspired by cortico-thalamo-cortical circuits, 2022.

Kai Li, Runxuan Yang, and Xiaolin Hu. An efficient encoder-decoder architecture with top-down attention for speech separation. In *International Conference on Learning Representations*, 2023.

Yi Luo and Nima Mesgarani. Conv-tasnet: Surpassing ideal time-frequency magnitude masking for speech separation. *IEEE/ACM Transactions on Audio, Speech, and Language Processing*, 27(8):1256–1266, 2019.

Yi Luo, Zhuo Chen, and Takuya Yoshioka. Dual-path rnn: efficient long sequence modeling for time-domain single-channel speech separation. In *2020-2020 IEEE International Conference on Acoustics, Speech and Signal Processing*, pp. 46–50. IEEE, 2020.

Héctor Martel, Julius Richter, Kai Li, Xiaolin Hu, and Timo Gerkmann. Audio-visual speech separation in noisy environments with a lightweight iterative model. In *Interppeech*. ISCA, 2023.

Ashesh D Mehta, Istvan Ulbert, and Charles E Schroeder. Intermodal selective attention in monkeys. ii: physiological mechanisms of modulation. *Cerebral cortex*, 10(4):359–370, 2000.

Nima Mesgarani and Edward F Chang. Selective cortical representation of attended speaker in multi-talker speech perception. *Nature*, 485(7397):233–236, 2012.

Lukas Mesik, Wen-pei Ma, Ling-yun Li, Leena A Ibrahim, ZJ Huang, Li I Zhang, and Huizhong W Tao. Functional response properties of vip-expressing inhibitory neurons in mouse visual and auditory cortex. *Frontiers in neural circuits*, 9:22, 2015.

Juan F Montesinos, Venkatesh S Kadandale, and Gloria Haro. Vovit: low latency graph-based audio-visual voice separation transformer. In *Proceedings of the European Conference on Computer Vision*, pp. 310–326. Springer, 2022.

Jennifer L Mozolic, Christina E Hugenschmidt, Ann M Peiffer, and Paul J Laurienti. Modality-specific selective attention attenuates multisensory integration. *Experimental Brain Research*, 184:39–52, 2008.

Risto Näätänen. The role of attention in auditory information processing as revealed by event-related potentials and other brain measures of cognitive function. *Behavioral and Brain Sciences*, 13(2):201–233, 1990.

James A O’sullivan, Alan J Power, Nima Mesgarani, Siddharth Rajaram, John J Foxe, Barbara G Shinn-Cunningham, Malcolm Slaney, Shihab A Shamma, and Edmund C Lalor. Attentional selection in a cocktail party environment can be decoded from single-trial eeg. *Cerebral Cortex*, 25(7):1697–1706, 2015.

Adam Paszke, Sam Gross, Francisco Massa, Adam Lerer, James Bradbury, Gregory Chanan, Trevor Killeen, Zeming Lin, Natalia Gimelshein, Luca Antiga, et al. Pytorch: An imperative style, high-performance deep learning library. volume 32, 2019.

Akam Rahimi, Triantafyllos Afouras, and Andrew Zisserman. Reading to listen at the cocktail party: multi-modal speech separation. In *Proceedings of the IEEE/CVF Conference on Computer Vision and Pattern Recognition*, pp. 10493–10502. IEEE, 2022.

Tommi Raij, Kimmo Uutela, and Riitta Hari. Audiovisual integration of letters in the human brain. *Neuron*, 28(2):617–625, 2000.

Kathleen S Rockland and Hisayuki Ojima. Multisensory convergence in calcarine visual areas in macaque monkey. *International Journal of Psychophysiology*, 50(1-2):19–26, 2003.

Olaf Ronneberger, Philipp Fischer, and Thomas Brox. U-net: Convolutional networks for biomedical image segmentation. In *MICCAI*, pp. 234–241. Springer, 2015.

Dmitry Ryumin, Denis Ivanko, and Elena Ryumina. Audio-visual speech and gesture recognition by sensors of mobile devices. *Sensors*, 23(4):2284, 2023.

Barry E Stein and Terrence R Stanford. Multisensory integration: current issues from the perspective of the single neuron. *Nature Reviews Neuroscience*, 9(4):255–266, 2008.

George Sterpu, Christian Saam, and Naomi Harte. Attention-based audio-visual fusion for robust automatic speech recognition. In *Proceedings of the 20th ACM International Conference on Multimodal Interaction*, pp. 111–115. ACM, 2018.

Cem Subakan, Mirco Ravanelli, Samuele Cornell, Mirko Bronzi, and Jianyuan Zhong. Attention is all you need in speech separation. In *2021-2021 IEEE International Conference on Acoustics, Speech and Signal Processing*, pp. 21–25. IEEE, 2021.

Quentin Summerfield. Lipreading and audio-visual speech perception. *Philosophical Transactions of the Royal Society of London. Series B: Biological Sciences*, 335(1273):71–78, 1992.

Emmanuel Vincent, Rémi Gribonval, and Cédric Févotte. Performance measurement in blind audio source separation. *IEEE Transactions on Audio, Speech, and Language Processing*, 14(4):1462–1469, 2006.

Jian Wu, Yong Xu, Shi-Xiong Zhang, Lian-Wu Chen, Meng Yu, Lei Xie, and Dong Yu. Time domain audio visual speech separation. In *2019 IEEE Automatic Speech Recognition and Understanding Workshop (ASRU)*, pp. 667–673, 2019.

A A. MODEL CONFIGURATIONS

We set the kernel size of the audio encoder and decoder to 2ms and the stride size to 1ms. The video encoder utilized a lip-reading pre-trained model consistent with CTCNet (Li et al., 2022) to extract visual vectors. The down-sampling times D for auditory and visual networks was set to 4, and the number of channels for all convolutional layers was set to 512. Moreover, the auditory and visual networks use the same set of weights in different cycles, respectively and they are cycled $N_F = 4$ times; the auditory-only networks were cycled $N_S = 12$ times. Furthermore, we proposed an optimized lightweight variant of SCANet, namely *SCANet-small*, which performed only $N_S = 6$ cycles on the auditory network and remarkably advanced the performance trade-off.. For the FFN in TCA block, we set three convolutional layers (512, 1024, 512), kernel size to (1, 5, 1), stride size to (1, 1, 1), and biases to (False, True, False). To avoid overfitting, we set the dropout probability for all layers to 0.1.

B B. TRAINING METHOD

Unlike previous AOSS (Luo & Mesgarani, 2019; Luo et al., 2020; Li et al., 2023) and AVSS methods (Wu et al., 2019; Li et al., 2022), our proposed SCANet estimates the signal-to-noise ratio (SNR) between the separated and original speech as the loss function. This is because the scale-invariant signal-to-noise ratio (SI-SNR) (Le Roux et al., 2019) causes the model to learn the physical direction of different signals while ignoring their energy differences, which may result in inconsistent energy between the separated audio and the original speech. The SNR for each speaker is defined as:

$$\mathcal{L}_{\text{SNR}} = 10 \cdot \log_{10} \left(\frac{\bar{\mathbf{A}}^2}{(\mathbf{A} - \bar{\mathbf{A}})^2} \right), \quad (6)$$

where \mathbf{A} and $\bar{\mathbf{A}}$ denote the target audio and the estimated audio, respectively.

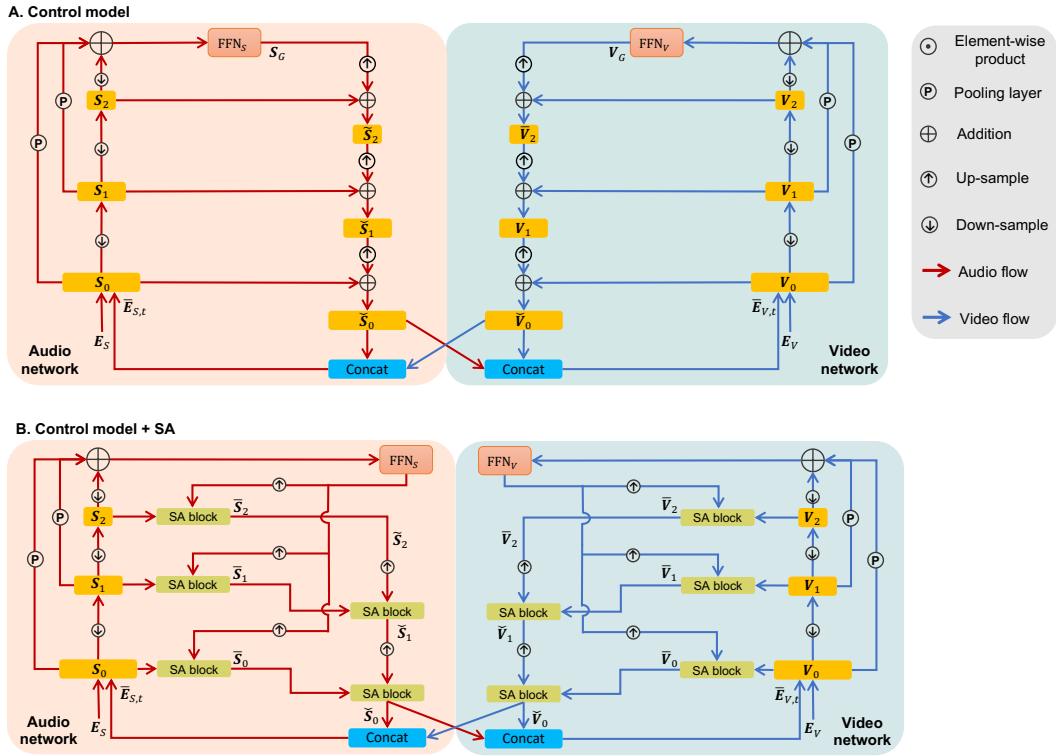


Figure S1: The overall pipeline of SCANet’s control models for audio-visual speech separation. (A) SCANet does not contain SA blocks or cross-attention blocks. (B) SCANet does not contain cross-attention blocks, only SA blocks.